Flexible and Transparent Plastic Electrodes Composed of Reduced Graphene Oxide/Polyaniline Films for Supercapacitor Application

Ashis K. Sarker and Jong-Dal Hong[*]

Department of Chemistry, Incheon National University, Incheon 406-772, Korea. [*]E-mail: hong5506@incheon.ac.kr

In this article, we described about the preparation and electrochemical properties of a flexible energy storage system based on a plastic polyethylene terephthalate (PET) substrate. The PET treated with UV/ozone was fabricated with multilayer films composed of 30 polyaniline (PANi)/graphene oxide (GO) bilayers using layer-by-layer assembly of positively charged PANi and negatively charged GO. The conversion of GO to the reduced graphene oxide (RGO) in the multilayer film was achieved using hydroiodic acid vapor at 100 °C, whereby PANi structure remained nearly unchanged except a little reduction of doping state. Cyclic voltammetry and charge/discharge curves of 30 PANi/RGO bilayers on PET substrate (shorten to PANi-RGO$_{30}$/PET) exhibited an excellent volumetric capacitance, good cycling stability, and rapid charge/discharge rates despite no use of any metal current collectors. The specific capacitance from charge/discharge curve of the PANi-RGO$_{30}$/PET electrode was found to be 529 F/cm^3 at a current density of 3 A/cm^3, which is one of the best values yet achieved among carbon-based materials including conducting polymers. Furthermore, the intrinsic electrical resistance of the PANi-RGO$_{30}$/PET electrodes varied within 20% range during 200 bending cycles at a fixed bend radius of 2.2 mm, indicating the increase in their flexibility by a factor of 225 compared with the ITO/PET electrode.

Key Words : Reduced graphene oxide, Polyaniline, Flexibility, Conductivity, Supercapacitor

Introduction

Currently, development of flexible and bendable energy storage devices has received strong attention in order to meet the next-generation electronic equipment including rollup displays and wearable devices.[1] Fabrication of bendable power sources is a major challenge due to a lack of reliable materials that combine electronically superior conductivity, high mechanical flexibility, and high stability in electrochemical environments. Over the past few years, carbon materials mixed with metal oxide and conducting polymers have been widely studied in supercapacitors. Supercapacitors are very attractive power sources, because their recharge times are generally short, they yield long life cycle, and high power. Graphene which is an emerging carbon material consisting of monolayered sp^2 hybird carbon atom, has been a hot topic for the use in flexible supercapacitor application owing to the good electronic conductivity, corrosion resistance in aqueous electrolyte and high mechanical elasticity.[2-5] Recently, conducting polymers including polyaniline (PANi), polypyrrole, polythiophene have been combined into graphene-based supercapacitors for the enhancement of total capacitance *via* an additional contribution of pseudo-capacitance.[6-9] Among the conducting polymers, PANi has been considered as one of the most promising electrode material due to its high flexibility and relatively high conductivity.[10] A large variety of composite materials including graphene and PANi has been developed for the supercapacitor application, *i.e.* graphene/PANi composite,[11] graphene/PANi nanofiber composite,[12] electrochemically polymerized PANi/

reduced graphene oxide (RGO) films,[13] PANi nanorods array on graphene oxide (GO) nanosheets,[14] graphene/PANi porous silica MCM-41,[15] and PANi-coated curved graphene active materials.[16] However, a challenging task still remains for development of flexible transparent lightweight supercapacitors with high power and energy density based on PANi/RGO film electrodes on a plastic substrates including polyethylene terephthalate (PET).

In this article, we report about a plastic-based supercapacitor fabricated with thin PANi/RGO films using layer-by-layer (LBL) deposition method,[17] which allows fine-tuning of morphology, thickness, and electric conductivity of the electrode material. The electrochemical properties of the plastic supercapacitor were evaluated using cyclic voltammetry (CV) and charge/discharge curves. We also investigated the stability in the electrical resistance of the PANi/RGO film on PET as a function of bending angle and cycles in comparison with indium tin oxide (ITO)/PET substrates.

Experimental Section

Materials. Natural graphite powder (particle size < 20 μm, 99.99%), PANi in emeraldine base form (MW 50 000), and hydroiodic acid (55%) were purchased from Sigma Aldrich, hydrochloric acid (35%) from Daejung Chemicals (South Korea), hydrogen peroxide (30%) from OCI Company Ltd. (South Korea), sulfuric acid (97%) from PFP Osaka (Japan), and ammonium hydroxide (29%) from Mallinckrodt Baker Inc. (NJ, USA), and were used as received. Transparent PET films were purchased from Saehan Industries (South

Korea), and fused silica was purchased from Maicom Quartz GmbH (Germany). ITO coated PET was purchased from i-one film (South Korea). All experiments and cleaning steps used the water from a Milli-Q Plus purification system (Millipore) with a resistivity of 18.2 MΩ·cm.

Methods. Synthetic method of GO and preparation of PANi solution were described in our previous paper.[6] Fused silica (12×45 mm^2), ITO (15×50 mm^2) and PET (15×50 mm^2) were used for LBL-assembly of the multilayer films composed of PANi/GO bilayers. Fused silica was cleaned by sonication in Piranha solution (sulfuric acid and hydrogen peroxide in 7:3 ration) at 70 °C for 1 h, and followed by sonication in RCA solution (water, hydrogen peroxide, and ammonium hydroxide in 5:1:1 ratio) at 70 °C for 1 h. In the case of ITO glass, the substrate cleaned by a successive rinsing in acetone, ethanol, and H$_2$O, was then dried under a gentle stream of nitrogen, and immersed into a freshly prepared piranha solution at RT just for 10 s. PET substrates (cleaned by a successive rinsing in acetone, ethanol, and H$_2$O) were then dried under a gentle stream of nitrogen and cleaned using Digital UV ozone system (PSD Series, Novascan) for 1 h for the removal of molecular organic contaminations and simultaneously the oxygenated functionalization of the surface by the irradiation of intense ultraviolet light; thereby, the cleaned PET substrates were negatively-charged.

For LBL-assembly of multilayer films based on dip-coating technique,[17] freshly cleaned substrates (fused silica, ITO and PET) were first immersed into a solution of positively charged PANi (0.5 mM, pH 2.6) for 15 min, and then washed in deionized water for 1 min. The washing step was repeated for three times. Subsequently, the substrates were dried under a gentle stream of nitrogen gas. Again, the PANi coated substrates were immersed into a solution of negatively-charged GO (0.125 mg/mL, pH 3.5) for 15 min to allow the deposition of the GO layer. The washing and drying steps as described above were followed. The LBL-assembly of PANi/GO bilayer on the substrate was repeated in a successive manner, until desired thickness of multilayer (PANi/GO) films was attained. The conversion of PANi/GO to PANi/RGO layer pairs in the multilayer films was achieved during being exposed to HI/H$_2$O vapor at 100 °C over 3 h. The LBL-assembly of PANi and GO onto a fused silica substrate was monitored using UV/visible spectrometer (Perkin Elmer, Lambda 40). The thickness of the multilayer film deposited on silicon wafers was measured using a real-time spectroscopic ellipsometer (EllipsoTechnology, Elli-SE-F) with a Xe arc lamp (350-820 nm) equipped with a rotating polarizer, a liquid cell with optical access at an incidence angle of 60°, and a multichannel detection system. Employing a self-made computer program, the elliptical azimuth and phase angle were calculated for both the cleaned reference substrate and the multilayer films. Field emission scanning electron microscopy (FE-SEM) was carried out on a JSM-7001F SEM microscope at an accelerating voltage of 20 kV. The structural characteristics of the multilayer films were investigated using Raman spectrometer (Raman-LTPL) at λ_{ex} of 533 nm. Elemental compositions of

the multilayer films were analyzed using X-ray photoelectron spectroscopy microprobe (PHI 5000 VersaProbe II, monochromatic AlKα X-rays source). The resistance of the samples was measured using the four and two probe method on KEITHLEY-2400.

The electrochemical measurement of the electrodes composed of 30 PANi/RGO bilayers (PANi-RGO$_{30}$) that were LBL-assembled on a non-conductive and flexible PET substrate (working electrode) were evaluated using cyclic voltammetry (CV), and galvanostatic charge/discharge measurement. The cell included platinum wire as the counter electrode and Ag/AgCl as the reference electrode in 1 M H$_2$SO$_4$ electrolyte.

Results and Discussion

Preparation of PANi/GO Multilayer Films. The LBL-assembly of GO and PANi layers was carried out on different solid substrates such as PET, indium tin oxide (ITO) and fused silica, according to our previous paper.[6] The pH of the PANi solution that yielded optimal doping conditions was found to be 2.6. The pH of the washing solution and GO solution were also set to 2.6 and 3.5, respectively, in order to minimize the transformation of the emeraldine salt into an emeraldine base. The deposition of PANi and GO on solid substrate PET was assessed based on the UV/visible absorbance. The deposition of up to alternating 15 PANi/GO bilayers was monitored by measuring the characteristic absorbance of the multilayer film at 550 and 830 nm, respectively, as shown in Figure 1 (inset), indicating the regular deposition of PANi and GO on the PET substrate. It is noteworthy that the FE-SEM topographical images of the PANi/RGO multilayer film on PET substrate obtained *via* HI/H$_2$O vapor treatment at 100 °C for 3 h (Figure S1), indicated no significant damage on the film surface.

Spectroscopic Studies of the Chemical Conversion from (PANi/GO) to (PANi/RGO) Films. GO in multilayer film composed of 30 PANi/GO bilayers (shorten to PANi-GO$_{30}$)
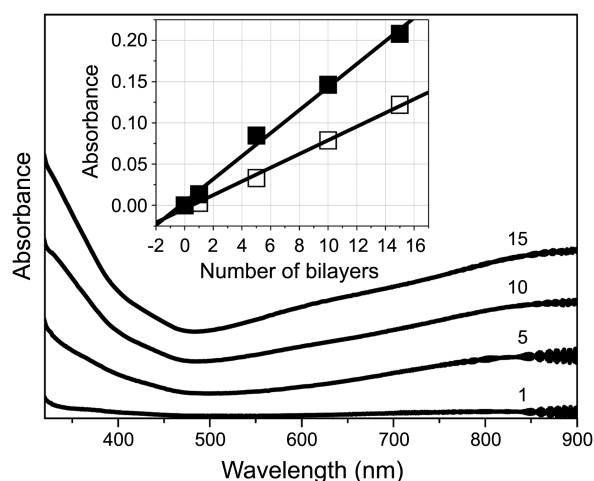

Figure 1. UV/visible absorption spectra of the multilayer films composed of different number of PANi/GO bilayers deposited onto a PET. Inset: Plot of the absorbance at 550 (□) and 830 nm (■) *vs.* the number of the bilayers.

was converted to RGO, as being exposed on HI/H$_2$O vapor at 100 °C for 3 h. The conversion from PANi/GO to PANi/RGO in a multilayer film during the HI/H$_2$O vapor treatment was investigated using UV/visible, Raman, and XPS spectroscopy.

The UV/visible spectra of a PANi-GO$_{30}$ multilayer film deposited onto a fused silica were compared before and after HI/H$_2$O vapor treatments, as shown in Figure 2. Note that UV/visible spectra of the pure GO and PANi films was also inserted in the supporting information (SI) for the references in the interpretation of overlapped absorbances of PANi-GO$_{30}$ film, as shown in Figure S2. The absorption peak at 232 nm, assigned to the π-π* transition of GO, was red-shifted to 280 nm, indicating an increased π-conjugation length due to the restoration of the delocalized electron system through elimination of oxygenated functional groups including carbonyl, carboxyl, epoxide, and hydroxyl on the GO upon exposure to HI/H$_2$O vapor.[18] The color of PANi-GO$_{30}$ films turned from blue to dark brown immediately after HI/H$_2$O vapor treatment (the digital images in insets of Figure 2), indicating the reduction of GO to RGO. The broad shoulder (290-350 nm) observed for GO was ascribed to the n-π* transition of epoxide (C-O-C) and peroxide (R-O-O-R) in the GO.[19] This broad shoulder was typically observed in solid-state GO thin films, indicating the presence of peroxide-like linkages (Figure S2a). The absorption at 200-500 nm was increased after the HI/H$_2$O vapor treatment, indicating the fact that conjugation (oxidation) state of pure PANi increased, while the absorption intensity in the range of 600 to 1100 nm was decreased due to slight reduction of doping state (Figure S2b). The HI/H$_2$O vapor reduction seems to have no significant effect on a broad absorbance (600-1100 nm) in the NIR region (centered at ~880 nm), which could be assigned to the dispersion of the polaron bands formed *via* overlap among the polarons of adjacent tetrameric units.[20,21] The bands were known to be particularly sensitive to the geometric arrangement of the polymer backbone. It is noteworthy that the characteristic absorbance of emeraldine base at 550 nm was not observed from PANi/RGO film (Figure 2), indicating that PANi still remains in a doping state. The characteristic absorbance of PANi/GO (310 nm) was shifted to 400 nm after HI/H$_2$O vapor treatment. The spectral shift was ascribed to the formation of a charge-transfer complex between the both PANi and RGO electron-rich components. The digital image of PANi-GO$_{30}$ film on PET depicted in Figure 2 (insets) showed high flexibility and also transparency of the electrodes that decreased from 67 to 44% after HI/H$_2$O vapor treatment (Figure S3). The ellipsometric thickness of PANi-GO$_{30}$ film was found to be 71.2 ± 1.4 nm. The thickness of the PANi-RGO$_{30}$ film decreased by about 3% upon chemical reduction using HI/H$_2$O vapor treatment and the ultimate thickness of PANi-RGO$_{30}$ film was 69.1 ± 2.2 nm.

The Raman spectra of PANi-RGO$_{30}$/fused silica film (Figure S4) illustrated the reduction from GO to RGO in the LBL-films during HI/H$_2$O vapor treatment. The GO/RGO reduction in the multilayer assemblies was clearly identified
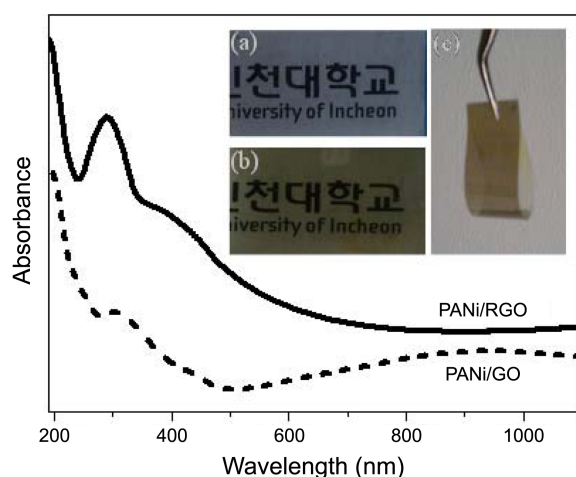

Figure 2. UV/visible absorption spectra of the multilayer films composed of PANi-GO$_{30}$ film (dash), which was converted to PANi-RGO$_{30}$ film by HI/H$_2$O vapor treatment at 100 °C (solid line). (Insets) The digital photo images of (a) PANi-GO$_{30}$/PET, (b) PANi-RGO$_{30}$/PET, and (c) Folded PANi-RGO$_{30}$/PET film.

by the increased D/G intensity ratio (1.17) compared to the ratio of the virgin films (0.90). The enhanced ratio of the D/G intensities resulted from the formation of more numerous new graphitic domains along with a decrease in the average size of the sp^2 domains upon reduction of the exfoliated GO.

The chemical compositions of the PANi-GO/PET analyzed using XPS were compared with those after the HI/H$_2$O vapor reduction, as shown in Figure 3. The composition of the multilayer films were calculated based on the areas of the XPS peaks, as listed in Table 1. High-resolution scan analysis of C, O, and N spectra (Figure 3(a)) allowed us to determine the composition of the virgin PANi/GO multilayer film: 73.5% C1s (284 eV), 23.4% O1s (532 eV), 3.1% N1s (399 eV), which were changed to 81.6%, 8.9%, and 7.6% after HI/H$_2$O vapor reduction, respectively. A distinctive feature of the composition analysis is the strong decrease in the oxygen content from 23.4 to 8.9% during the HI/H$_2$O vapor reduction, exhibiting considerable deoxygenation from GO layers. Besides, surface analysis was performed by fitting the XPS curve to a Gaussian-Lorentzian function after correction for Shirley background.[22] Deconvolution of C 1s peak (Figure 3b) revealed four characteristic peaks of C-C/C=C (283.5 eV), C-O (286.0 eV), C=O (287.5 eV), and O-C=O (289 eV), indicating the presence of oxygenated functional groups on the GO sheets.[23] All oxygenated functional groups containing characteristic peaks of C-O (286.0 eV), C=O (287.5 eV), and O-C=O (289 eV) were decreased significantly after HI/H$_2$O vapor treatment (Figure 3(c)). Note that the C:O ratio in the composition of GO were comparable to the literature values,[24] despite batch-to-batch variability in the composition of functional groups in GO samples. The N1s core-level spectra (Figure 3(d) and 3(e)) revealed three peaks in the deconvolution of the spectra, which were corresponded to different electronic states: The benzenoid amine with a binding energy (BE) centered at 398.9 eV, the quinoid amine with a BE at 397.5 eV, and the
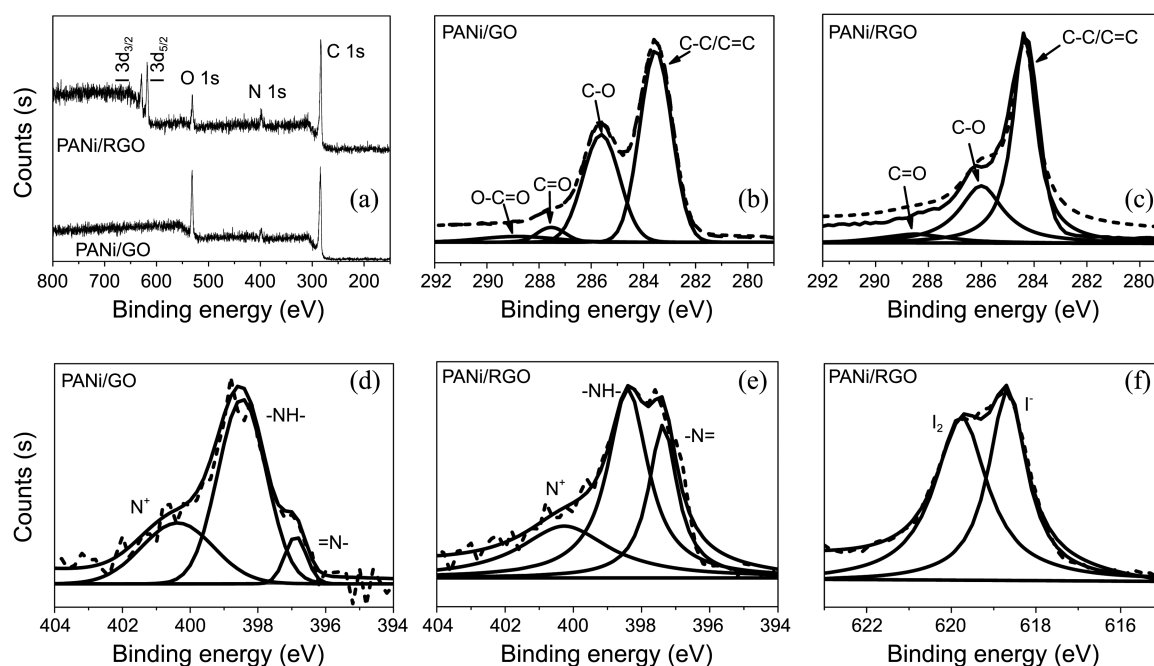
Figure 3. XPS spectra of the PANi/GO and PANi/RGO films. (a) Survey scan, (b, c) C 1s, (d, e) N 1s and (f) I $3d_{5/2}$ spectra.

nitrogen cationic radical (N^+) with a BE at 401.0 eV.[13] The benzenoid amine (-NH-) content decreased from 62.3 to 46.3%, while the nitrogen quinoid amine (-N=) increased significantly from 7.1 to 27.0%. The cationic radical (N^+) content also decreased slightly from 30.5 to 26.6% (Table 1). These observations indicate that the oxidation level of PANi in the multilayer films was strongly enhanced during HI/H_2O vapor reduction of the PANi/GO films. It should be noted that trace amounts (1.9%) of I was detected from the PANi/RGO$_{30}$ films. The iodine anions were expected to play an essential role to reduce GO and the formation of conjugated RGO.[25] The I $3d_{3/2}$ and I $3d_{5/2}$ core-level spectra revealed two peaks in the deconvolution of the spectra, which were corresponded to different electronic states: the I $3d_{3/2}$ with a binding energy (BE) centered at 630 eV and the I $3d_{5/2}$ with a BE at 619 eV (Figure 3(a)). From the $d_{5/2}$ peak, the iodine (I_2) and iodide ion (I^-) content were found to be 53.4% and 46.5%, respectively (Figure 3(f)). These residual iodine anion (I^-) and neutral iodine (I_2) acted as dopants in the conjugated PANi and RGO layers.[25,26]

Electrochemical Properties. The electrochemical performance of PANi-RGO$_{30}$ electrodes LBL-assembled on a PET substrate (working electrode) were evaluated in a cell including a platinum wire (counter electrode) and an Ag/AgCl (reference electrode) in 1 M H_2SO_4 electrolyte with

using CV, and galvanostatic charge/discharge measurements. By comparison, the evaluation measurements were also carried out for PANi-RGO$_{30}$ on ITO-coated PET substrate (the current collector).

The average volumetric capacitance values, C (F/cm³) of the electrodes were estimated based on the galvanostatic charge/discharge process, according to the following Eqs. (1), as summarized in Table 2.

$$C = (I \cdot \Delta t)/(\Delta E \cdot V) \qquad (1)$$

where I is the current loaded (A), Δt is the discharge time (s), ΔE is the potential change during the discharge process (volt), and V is the volume of the active material in electrode (cm³).

Rate-dependent CVs for the PANi-RGO$_{30}$/PET electrode (Figures 4(a)) showed almost rectangular-shaped curve for all scan rates from 5 to 40 mV/s over potential range of −0.2~0.8 V, indicating the high conductivity of the electrode and the optimal capacitive behavior. Representative curves in the charge/discharge plot of the PANi-RGO$_{30}$/PET electrodes at current density from 3 to 20 A/cm³ (Figure 4(b)) showed the near-triangular shape, indicating less mass transport resistance and good charge propagation of ions within the electrodes. The specific capacitance from charge/discharge curve of PANi-RGO$_{30}$/PET electrode was found to be 529 F/cm³ at current density 3 A/cm³ (Table 2), which is one of the best values yet achieved among carbon based materials including conducting polymers listed in Table S1. The electrode potential in the discharge curve decreased exponentially in distinctive two stages of the potential drop; first sharply in the range of 0.8~0.5 V and then gently in the range of 0.50~(−0.2) V. The former stage with relatively short discharge duration is ascribed to pure electric double layer (EDL) capacitance. The latter stage with much longer

Table 1. The composition (%) of high resolution C 1s and N 1s peaks in XPS of the LBL-assembled PANi/GO and PANi/RGO films

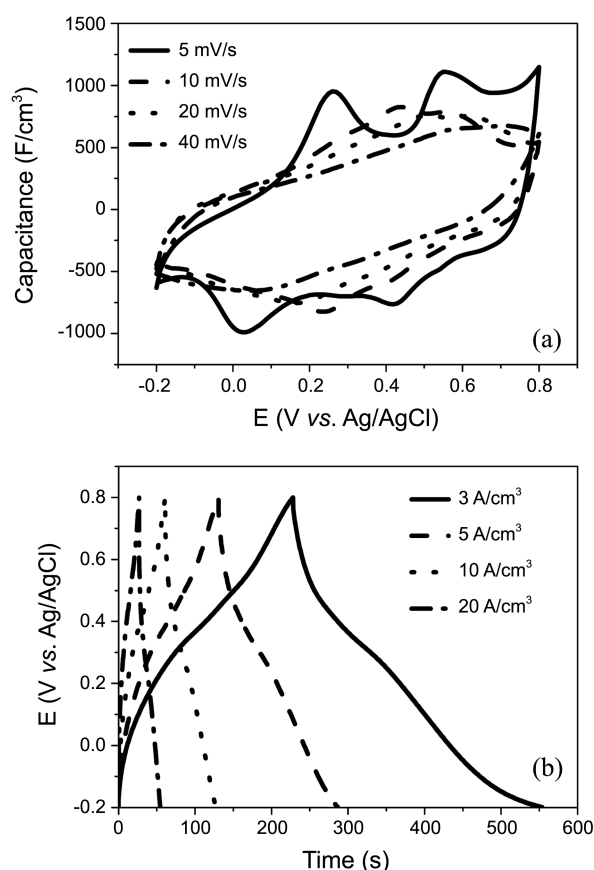| Samples	C-C 283.5	C-O 286	C=O 287.8	O-C=O 289.5	=N– 397.5	–NH– 398.9	N^+ 401.0
PANi/GO	56.29	36.15	3.74	3.80	7.1	62.3	30.5
PANi/RGO	61.0	31.21	7.78	–	27.0	46.3	26.6

Figure 4. (a) Cyclic voltammograms at scan rate of 5-40 mV/s (b) Galvanostatic charge/discharge curves at current density of 3-20 A/cm^3 of PANi-RGO$_{30}$/PET.

Table 2. Volumetric capacitances calculated from charge/discharge curves of PANi-RGO$_{30}$/PET and PANi-RGO$_{30}$/ITO

Current Density (A/cm^3)	3	5	10	20	30	50	70
Capacitance (F/cm^3)/PET	529	422	358	299	264	199	136
Capacitance (F/cm^3)/ITO	956	783	662	573	526	461	416
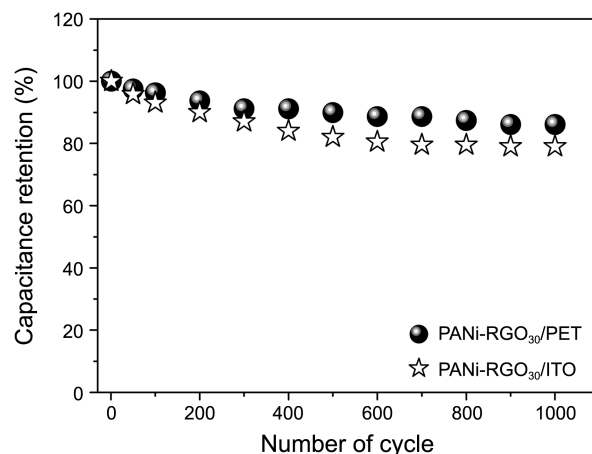
Figure 5. Cycle stability tests of PANi-RGO$_{30}$/PET and PANi-RGO$_{30}$/ITO electrode.

discharge duration was faradaic capacitance of the PANi component.[27] For instance, Zhiqiang Niu and co-workers observed a specific capacitance of 359 F/cm^3 at 5 mV/s with a flexible RGO electrode on PET substrate.[28]

Meanwhile, PANi-RGO$_{30}$/ITO showed no distinctive faradaic current peaks compared to PANi-RGO$_{30}$/PET, but higher EDLC contribution to the CV (Figure S5). The different capacitive behavior was resulted mainly from higher conductivity of the current collector ITO compared to PET. The redox peaks in CV of PANi-RGO$_{30}$/ITO could not be clearly identified, because they were supposedly overlaid by the strong EDL capacitive current, which relies highly on conductivity of the electrode (Figure S5). The specific capacitance from charge/discharge curve of PANi-RGO$_{30}$/ITO/PET electrode was found to be 956 F/cm^3 (Table 2) which was higher than that of PANi-RGO$_{30}$/PET electrode. The maximum volumetric capacitance of PANi-RGO$_{30}$/PET and PANi-RGO$_{30}$/ITO electrodes decreased exponentially as the current density increased, leading to the values of 136 and 416 F/cm^3 at 70 A/cm^3, respectively (Table 2).

The durability of the electrode materials is extremely important for the long-term maintenance of supercapacitors. The maximum specific capacitance of the PANi-RGO$_{30}$/PET electrode decreased gently even after 1000 charge/discharge cycles at a current density of 3 A/cm^3, compared to PANi-RGO$_{30}$/ITO (14 *vs.* 21%), as shown in Figure 5. The PANi-

RGO$_{30}$/PET exhibited an excellent volumetric capacitance, good cycling stability, and rapid charge/discharge rates, which are required for supercapacitors. Furthermore, PANi/GO and PANi/RGO films were strongly adhered on PET, so that the films could not be stripped off easily from the substrate even by applying mechanical force. By contrast, PANi/GO and PANi/RGO films were peeled off easily from ITO and fused silica.

Flexibility of PANi-RGO$_{30}$/PET Electrode. The combination of excellent mechanical flexibility and electric capacitive performance is the key to realizing flexible energy storage devices.[29] Although constructing specific structural layouts and developing new electronic materials are conceptually different topics, they also offer complementary ways to achieve flexible electronics.[30] The excellent electrical and mechanical properties of the organic PANi/RGO thin films and the unique network structure of PANi/RGO multilayer films would provide the composite electrode great potential use in flexible conductors; a key component of flexible and curvilinear large-area electronics such as sensory skins for robotics, structural health monitors, and wearable communication devices.

The electrical resistance of the PANi-RGO$_{30}$/PET was determined as a function of the bending angle, and compared with that of ITO/PET electrode (Figure 6). The bend test was carried out using a home-made two-point bending device and a high-precision mechanical system. The electrical resistance of the PANi-RGO$_{30}$/PET was increased gently up to a bend radius of 2.2 mm, and recovered to the initial value after straightening (Figure 6(a)). The PANi-RGO$_{30}$/PET electrode exhibited a weak tendency to increase in the resistance after the first three cycles. The electrical resistance
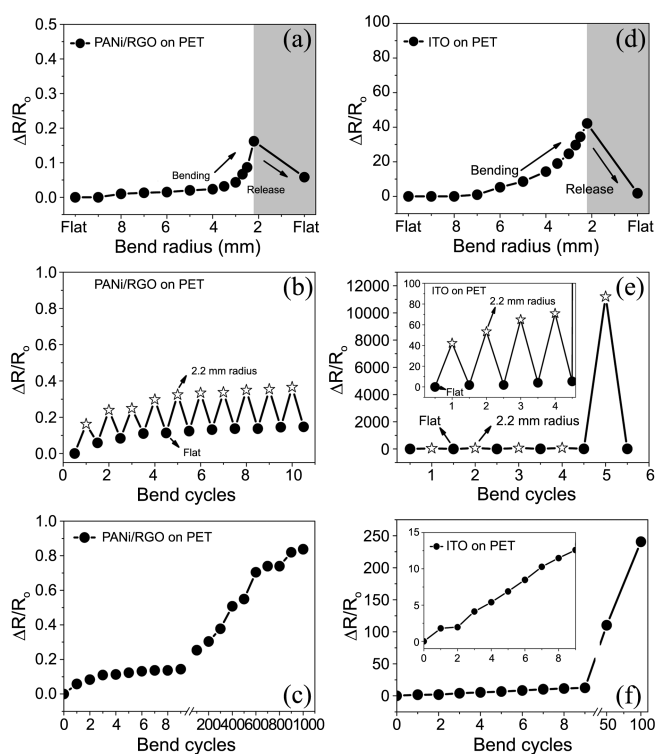
Figure 6. Electric resistance change of thin films under mechanical deformation. Electric resistance variation of thin films at a bend radius up to 2.2 mm in the first cycle (a) PANi-RGO$_{30}$/PET, (d) ITO on PET. Electric resistance change of the films when bending to a radius of 2.2 mm and then straightening for each cycle (b) PANi-RGO$_{30}$/PET, (e) ITO on PET. The resistance change of the films as a function of bend cycles for a bend radius of 2.2 mm (c) PANi-RGO$_{30}$/PET, (f) ITO on PET.

difference of the PANi-RGO$_{30}$/PET electrode per each bend/straight cycle remains nearly unchanged within 20% (Figure 6(b)). The resistance of the PANi-RGO$_{30}$/PET tended to increase strongly after 200 bending cycles with a fixed bend radius of 2.2 mm (Figure 6(c)). Conventional current collectors in supercapacitors including metallic foils and thin films tend to possess poor mechanical robustness and elasticity despite higher electrical conductivity,[29] which make them unsuitable for flexible conductors. For example, ITO on a flat PET sheet showed a low sheet resistance of 150 ohm, which, however, strongly increased upon slight bending (Figure 6(d) and 6(e)). The resistance of ITO/PET electrode increased about 200% even after 1 bending cycle (Figure 6(f)). The ultimate flexibility of the PANi/RGO thin films increased by a factor of 225 compared with the ITO.

Conclusion

Highly stable PANi/GO thin films were deposited onto a plastic substrate using LBL electrostatic self-assembly method. The GO in PANi/GO thin films on PET substrate were reduced to RGO by HI/H$_2$O vapor treatment at 100 °C, whereby PANi structure remained nearly unchanged except a little reduction of doping state. The Raman spectra of PANi-RGO$_{30}$/fused silica film (Figure S4) clearly identified

the reduction from GO to RGO in the LBL-films during the HI/H$_2$O vapor treatment based on the increased D/G intensity ratio (1.17) compared to the ratio of the virgin films (0.90). A distinctive feature of the composition analysis using XPS was the strong decrease in the oxygen content from 23.4% to 8.9% during the HI/H$_2$O vapor reduction process, exhibiting considerable deoxygenation from GO layers. The characteristic absorbance of PANi/GO at 310 nm was red-shifted to the longer wavelength of 400 nm in UV/visible spectra of PANi/RGO multilayer film after HI/H$_2$O vapor treatment. The spectral shift was ascribed to the formation of a charge-transfer complex between the electron-rich components; PANi and RGO.

The electrodes fabricated using ultrathin PANi/RGO films exhibited a specific capacitance of 529 F/cm^3 (at a current density of 3 A/cm^3), and achieved a new record value among carbon-based devices including conducting polymers on a flexible PET substrate.

Furthermore, the electrical resistance of the PANi-RGO$_{30}$/PET electrodes remained nearly unchanged within 20% during 200 bending cycles with a fixed bend radius of 2.2 mm, indicating the increase in their flexibility by a factor of 225 compared with the ITO/PET electrode. The PANi-RGO$_{30}$/PET capacitors exhibited an improved cycling stability (14 *vs.* 21%) after 1000 charge/discharge cycles at a current density of 3 A/cm^3, compared to PANi-RGO$_{30}$/ITO. In addition, PANi/GO and PANi/RGO films showed much stronger adhesive affinity on PET, compared to ITO surface. The LBL-assembly method was shown to provide not only a tool to prepare well-organized homogeneous PANi/RGO composites, but also optimal oxidation state of PANi in the multilayer films for achieving excellent electronic conductivities. The results we achieved in this study demonstrated potential application of PANi-RGO/PET electrodes in flexible and foldable supercapacitors.

References

1. Gwon, H.; Kim, H. S.; Lee, K. U.; Seo, D. H.; Park, Y. C.; Lee, Y. S.; Ahn, B. T.; Kang, K. *Energy Environ. Sci.* **2011**, *4*, 1277.
2. Clark, K.W.; Zhang, X. G.; Vlassiouk, I. V.; He, G. W.; Feenstra, R. M.; Li, A. P. *ACS Nano* **2013**, *7*, 7956.
3. Chen, S.; Brown, L.; Levendorf, M.; Cai, W.; Ju, S. Y.; Edgeworth, J.; Li, X.; Magnuson, C. W.; Velamakanni, A.; Piner, R. D.; Kang, J. Y.; Park, J.; Ruoff, R. S. *ACS Nano* **2011**, *5*, 1321.
4. Singh, B. P.; Nayak, S.; Nanda, K. K.; Jena, B. K.; Bhattacharjee, S.; Besra, L. D. *Carbon* **2013**, *61*, 47.
5. Scarpa, F.; Adhikari, S.; Phani, A. S. *Nanotechnology* **2009**, *20*, 065709.
6. Sarker, A. K.; Hong, J. D. *Langmuir* **2012**, *28*, 12637.
7. Sarker, A. K.; Hong, J. D. *Colloids and Surfaces A: Physicochem. Eng. Aspects* **2013**, *436*, 967.
8. Oliveira, H. P.; Sydlik, S. A.; Swager, T. M. *J. Phys. Chem. C* **2013**, *117*, 10270.
9. Alvi, F.; Ram, M. K.; Basnayaka, P.; Stefanakos, E.; Goswami, Y.; Hoff, A.; Kumar, A. *ECS Trans.* **2011**, *35*, 167.

10. Wang, Y. G.; Li, H.Q.; Xia, Y. Y. *Adv. Mater.* **2006**, *18*, 2619.
11. Yan, J.; Wei, T.; Shao, B.; Fan, Z.; Qian, W.; Zhang, M.; Wei, F. *Carbon* **2010**, *48*, 487.
12. Zhang, K.; Zhang, L. L.; Zhao, X. S.; Wu, J. *Chem. Mater.* **2010**, *22*, 1392.
13. Feng, X. M.; Li, R. M.; Ma, Y. W.; Chen, R. F.; Shi, N. E.; Fan, Q. L. W. *Adv. Funct. Mater.* **2011**, *21*, 2989.
14. Zhang, S.; Zeng, M.; Xu, W.; Li, J.; Xu, J.; Wang, X. *DaltonTrans.* **2013**, *42*, 7854.
15. Feng, X.; Yan, Z.; Chen, N.; Zhang, Y.; Liu, Z.; Ma, Y.; Yang, Z.; Hou, W. *New J. Chem.* **2013**, *37*, 2203.
16. Chen, W.; Rakhi, R. B.; Alsharref, H. N. *Nanoscale* **2013**, *5*, 4134.
17. Decher, G.; Hong, J. D. *Ber. Bunsen-Ges. Phys. Chem.* **1991**, *95*, 1430.
18. Li, D.; Müller, M. B.; Gilje, S.; Kaner, R. B.; Wallace, C. G. *Nat. Nanotechnol.* **2008**, *3*, 101.
19. Saxena, S.; Tyson, T. A.; Shukla, S.; Negusse, E.; Chen, H. Y.; Bai, J. M. *Appl. Phys. Lett.* **2011**, *99*, 013104.
20. Fu, Y.; Weiss, R. A. *Synth. Met.* **1997**, *84*, 129.
21. Liu, C.; Zhang, J.; Shi, G.; Chen, F. *J. Appl. Polym. Sci.* **2004**, *92*, 171.
22. Yang, D. X.; Velamakanni, A.; Bozoklu, G.; Park, S. J.; Stoller, M.; Piner, R. D.; Stankovich, S.; Jung, I. H.; Field, D. A.; Ventrice, C. A., Jr.; Ruoff, R. S. *Carbon* **2009**, *47*, 145.
23. Mattevi, C.; Eda, G.; Agnoli, S.; Miller, S.; Mkhoyan, K. A.; Celik, O.; Mastrogiovanni, D.; Granozzi, G.; Garfunkel, E.; Chhowalla, M. *Adv. Funct. Mater.* **2009**, *19*, 2577.
24. Byon, H. R.; Lee, S. W.; Chen, S.; Hammond, P. T.; Horn, Y. S. *Carbon* **2011**, *49*, 457.
25. Pei, S. F.; Zhao, J. P.; Du, J. H.; Ren, W. C.; Cheng, H. M. *Carbon* **2010**, *48*, 4466.
26. Sharma, S. N. *Mater. Chem. Phys.* **2006**, *100*, 345.
27. Wu, Q.; Xu, Y.; Yao, Z.; Liu, A.; Shi, G. *ACS Nano* **2010**, *4*, 1963.
28. Niu, Z.; Zhang, L.; Liu, L.; Zhu, B.; Dong, H.; Chen, X. D. *Adv. Mater.* **2013**, *25*, 4035.
29. Sekitani, T.; Noguchi, Y.; Hata, K.; Fukushima, T.; Aida, T.; Someya, T. *Science* **2008**, *321*, 1468.
30. Rogers, J. A.; Someya, T.; Huang, Y. G. *Science* **2010**, *327*, 1603.